Cement and Concrete Research 152 (2022) 106679

Contents lists available at ScienceDirect

Cement and Concrete Research

journal homepage: www.elsevier.com/locate/cemconres

Numerical approach to pipe flow of fresh concrete based on MPS method

Zhisong Xu, Zhuguo Li *, Fei Jiang

Graduate School of Science and Technology for Innovation, Yamaguchi University, Ube, Yamaguchi, Japan

ARTICLE INFO

Keywords:
Numerical simulation
Fresh concrete
Pipe flow
MPS
Slip layer
Segregation
Coarse aggregate

ABSTRACT

As a fundamental study of concrete pumping, this study developed a numerical method to simulate the flow and segregation of fresh concrete in pipes, based on the improved MPS (Moving Particle Semi-implicit) that has complete implicit algorithm, hereafter called I-MPS. The slip layer (LL) near the pipe inner wall was treated by the macroscopic approach, which estimates the slip resistance and the volumetric flow rate of LL from the apparent slip velocity of LL. Two constituent models were used to describe fresh concrete, called single-phase & mono-particle (SPMP) model and double-phase & multi-particle (DPMP) model, respectively. In the former, fresh concrete is considered as a single-phase granular fluid, but in the latter, fresh concrete is regarded as two-phase granular fluid with different particle shapes and sizes of coarse aggregate and matrix mortar. By comparing the numerical and theoretical pumping pressures of three concretes having slump from 13 cm to 21 cm, it was found that by using the macroscopic approach of LL and either of the constituent models, the numerical approach can predict properly the pumping pressure and velocity profile of fresh concrete in pipes. Moreover, if using the DPMP model, the segregation behavior of coarse aggregate particles during the pipe flow can also be simulated.

1. Introduction

Concrete pumping has become one of the most widely used method to transport concrete. This method can greatly improve the construction efficiency, consequently reducing construction cost, and allowing concrete to be cast in difficult-to-access locations. The use of the pumping method will continue to grow due to the increased demand for large-scale concrete structures such as high-rise building and long-span bridge. However, some problems may occur during pumping, among which insufficient pumping pressure and weak pumpability of fresh concrete (including pipe blockage, segregation) are the most serious issues [1,2].

When fresh concrete is regarded as a Bingham fluid with yield stress, the Buckingham-Reiner equation [3] may be used to predict pressure required for concrete to flow through a pipe. However, it is found that the Buckingham-Reiner equation leads to an overestimation of pumping pressure at certain volumetric flow rates [4]. This is primarily due to the formation of slip layer (also referred to as a boundary layer or lubrication layer) near the inside wall of pipe, which reduces the pumping pressure. With consideration of slip layer (LL), several pressure prediction models were recently developed, such as Kaplan's model [5], Choi's model [6], Kwon's model [2], and Mechtcherine's model [7], etc. These models incorporate the rheological properties of not only the bulk concrete, but also the slip layer. Besides the pumping pressure, other concern about concrete pumping is the segregation of aggregate, which is a main reason of pipe blockage. As mentioned earlier, the slip layer plays a dominant role during pumping, which is formed by the migration of large aggregate particles towards the low shear rate zone. It is considered that coarse aggregate particles undergo the shear-induced migration towards the inner, while cement paste and finer aggregate particles move towards the pipe wall [6,8,9]. Also, in front of the concrete, the concentration of coarse aggregate is high, even a plug of coarse aggregates is caused [1,10]. Thus, the segregation prediction of pumped concrete is also an important issue.

In many construction sites and guidelines, the pumpability of fresh concrete is qualitative assessed based on the slump test. However, for concrete pumping, the shear strain rate is typically around 10 s^{-1} to 100 s^{-1}, whereas, for the slump test, it is only 1 s^{-1} or less [11]. At such low shear strain rate, the result of slump test does not encapsulate the effects of dynamic segregation and slip layer on the pumping behavior of concrete. Hence, the slump test may not be relevant for predicting the ability of concrete to flow in a pipe. Moreover, with the development of concrete's admixtures, the rheological properties of fresh concrete, such as self-compacting concrete (SCC) and high-performance concrete (HPC), are very different from conventional concrete [12], so that the knowledge and the guidelines of concrete pumping for conventional

* Corresponding author.
E-mail address: li@yamaguchi-u.ac.jp (Z. Li).

https://doi.org/10.1016/j.cemconres.2021.106679
Received 11 July 2020; Received in revised form 25 August 2021; Accepted 22 November 2021

concrete may be no longer applicable to new types of concrete [4]. Consequently, the development of prediction technology of concrete pumpability has been becoming an important issue for the concrete industry. If the pumping behavior of concrete mixture can be accurately predicted from its rheological properties, and other aspects of pumpability, such as dynamic segregation of coarse aggregate and slump loss, can be assessed, then concrete mixture can be optimized in the laboratory.

Although pumping experiment of concrete is able to evaluate the pump pressure [13–17], the experiment needs quite amount of materials and labor, vertical pumping experiment is very difficult, and it is almost impossible to observe segregation behavior of aggregate particles due to the invisibility of internal flow. The commercial CFD software is usually employed to simulate the pipe flow to predict the velocity distribution and pressure loss. However, fresh concrete is considered as single-phase fluid in CFD methods, it is unable to provide information about the dynamic segregation of concrete in pipe for predicting blockage [9,11,18]. Recently, the meshless particle method, such as Smoothed Particle Hydrodynamics (SPH) method [19], has been increasingly used in the flow simulation of fluid, which represents the fluid with particles. The meshless particle method has the potential to numerically discuss aggregate segregation [20].

The SPH method has been proved to be applied to the flow simulation of fresh concrete [21–24]. There is no doubt that accurate calculation of pressure is important for the pumping simulation. However, since in the SPH the ideal equation of state is usually used to calculate the pressure, the compression of fluid particles will occur under high pumping pressure. And since the magnitude of time step is limited in the SPH, the accuracy and efficiency of calculation are greatly reduced. For analyzing incompressible fluid problem, Koshizuka [25] developed a new meshless method named Moving Particle Semi-implicit (MPS). The MPS has been successfully used in the simulation of multiphase flows under high pressure [26], and the flow simulations of fresh cementitious fluid [27]. In the original MPS, since an explicit algorithm is used for the viscous item, the time step needs to be set very small to stabilize the calculation results for a fluid with high viscosity, such as fresh concrete [28], accordingly the calculation efficiency of MPS is reduced. For this reason, the authors developed a complete implicit MPS (I-MPS) method [29], and confirmed it to be more applicable to the flow simulation of fresh concrete. Now there is no meshless particle method that predicts the pressure loss together with the segregation behavior of pumped concrete. It is urgent to establish a numerical model for concrete pumping based on the flow characteristics of fresh concrete in pipe.

As a fundamental study on the numerical prediction technology of pumpability of fresh concrete, in this study, a new numerical simulation method for the pipe flow of concrete was proposed based on the I-MPS. In this numerical approach, the tribological behavior model [4,16,30] was adopted to describe the shear resistance of slip layer, and two types of constituent models, named single-phase & mono-particle (SPMP) model and double-phase & multi-particle (DPMP) model [31], were used to describe fresh concrete. The former expresses fresh concrete with spherical fluid particles having same size and density. But in the latter, fresh concrete is regarded as two-phase granular fluid of matrix mortar and coarse aggregate, and the coarse aggregate particles are composed of elementary particles so as to have different sizes and random shapes.

After the discussion on the reasonable size of elementary particle and the effect of the thickness of slip layer on the vertical pipe flow simulation, pumping pressure-volumetric flow rate relationships and velocity profiles were investigated numerically by using the proposed numerical approach. By compared with the theoretical pumping pressure for three series of concrete with different slump values, the proposed numerical approach to pipe flow of fresh concrete was validated. The dynamic coarse aggregate segregation behavior was also discussed by using the DPMP model.

2. Numerical simulation method of fresh concrete pipe flow

2.1. Algorithm of I-MPS

In this study, numerical method of pipe flow was developed based on the complete implicit MPS (I-MPS). The I-MPS not only solves the compression problem of discrete particles occurring in the general SPH, but also it is more efficient and gives more stable computational results than the original MPS due to the uses of complete implicit algorithm and high ordered Laplacian model [29]. The governing equations of I-MPS are the conservation laws of mass and momentum, as follows:

$$\frac{1}{\rho}\frac{d\rho}{dt}+\nabla\cdot\vec{u}=0,\frac{d\vec{u}}{dt}=-\frac{1}{\rho}\nabla P+\frac{\mu}{\rho}\nabla^2\vec{u}+\vec{g} \tag{1}$$

where, ρ is density of fluid, $\vec{u}$ is velocity, t is time, P is pressure, $\vec{g}$ is gravitational acceleration, and μ is dynamic viscosity of fluid.

The former, called conservation law of mass, describes the change of density with the elapsed time, and the latter, called conservation law of momentum, expresses the fluid motion under pressure, viscous force, and gravity. Only gravity is considered as external force, whereas pressure and viscous force are treated as interaction between neighboring particles. Since the I-MPS treats fluid as incompressible, the derivative of density ρ with respect to time t is equal to 0.

Though the meshless particle methods, such as SPH and MPS, treat fluid with discrete particles, the particles have no size in term of mathematical concept. In order to facilitate the description of particles in the flow simulation output, the fluid particles are imaged as spheres with same size, thus the diameter of sphere is equal to the inter-particle distance. Physical quantities are defined for the particles, and their derivatives are calculated based on the weight function. The weighted average of interactions between the analyzed particle and other particles in the influence domain (as shown in Fig. 1) is performed, and the weight function (kernel) employed in the I-MPS is shown in the following.

$$w(r_{ij})=\begin{cases}\dfrac{r_e}{r_{ij}}-1, & 0<r_{ij}<r_e\\ 0, & r_{ij}\geq r_e\end{cases},r_{ij}=\left|\vec{r}_j-\vec{r}_i\right| \tag{2}$$

where, r_{ij} is distance between two particles, and r_e is radius of influence domain.

Generally, the larger the influence domain considered, the higher the calculation accuracy, but it will greatly reduce the calculation efficiency. For raising the calculation efficiency and stabilizing of the calculation results, r_e is recommended to be 2–4 times of the distance between particle centers [25]. Thus, the radius (r_e) of influence domain was set as 2.1 times of particle center distance in case of gradient $\nabla\phi$, while the r_e of the circle domain was set as 4.1 times of particle center distance when calculating the Laplacian operator $\nabla^2\phi$.

The flowchart of I-MPS algorithm is shown in Fig. 2. In the beginning of time-step k, the position, velocity and pressure of particle i are noted

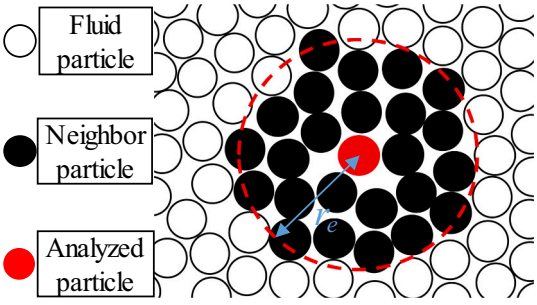

Fig. 1. Influence domain of analyzed particle.

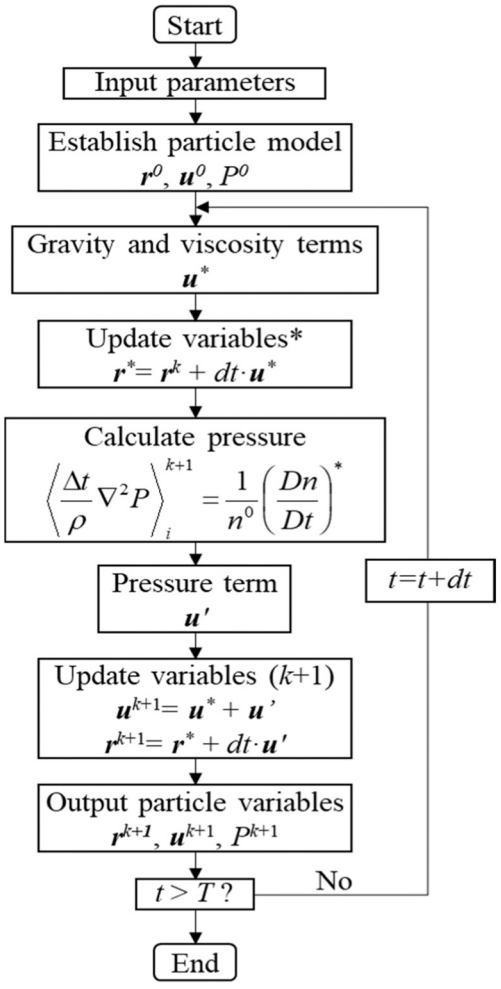

Fig. 2. Flowchart of I-MPS algorithm.

as $\langle \vec{r} \rangle_i^k$, $\langle \vec{u} \rangle_i^k$, and $\langle P \rangle_i^k$, respectively. After considering the gravity and viscosity terms, the position and velocity are updated to the temporary values $\langle \vec{r} \rangle_i^*$ and $\langle \vec{u} \rangle_i^*$, and the pressure $\langle P \rangle_i^{k+1}$ in the end of time-step k or in the beginning of next time-step $k+1$ can be obtained by solving the pressure Poisson equation based on the temporary values. The velocity and position of the particle i in the end of time-step k are corrected by using the pressure gradient to get $\langle \vec{u} \rangle_i^{k+1}$ and $\langle \vec{r} \rangle_i^{k+1}$, which are initial velocity and position of the particle i at next time-step $k+1$.

In the I-MPS, implicit calculations are used to solve the viscosity term and to calculate the pressure so as to improve the calculation efficiency and accuracy. The implicit expressions are shown as follows:

$$\langle \vec{u} \rangle_i^k + dt \cdot \langle \frac{\mu}{\rho}\nabla^2 \vec{u} \rangle_i^* = \langle \vec{u} \rangle_i^* \tag{3}$$

$$\langle \frac{dt}{\rho}\nabla^2 P \rangle_i^{k+1} = \frac{1}{n^0}\left(\frac{dn_i}{dt}\right)^* \tag{4}$$

The Conjugate Gradient (CG) solver was used for the above linear algebraic equations. The Laplacian in the Poisson equation of Eqs. (3) and (4) is discretized by higher order Laplacian (HL) scheme [32] as:

$$\langle \nabla^2 \phi \rangle_i = \frac{5-d}{n^0}\sum_{j \neq i}(\phi_j - \phi_i)\frac{r_e}{\left|\vec{r}_j^* - \vec{r}_i^*\right|^3} \tag{5}$$

where, ϕ represents variations, d is model dimension and equals to 3 in three-dimensions. n^0 is a constant representing the initial particle number density.

The gradient term of I-MPS is a radial function. To ensure the stability of the numerical results, a corrected gradient discretization [33] was used. ϕ_i' is used in place of ϕ_i, as the configuration of neighboring particles is not isotropic in general. The corrected gradient equation is shown as:

$$\langle \nabla \phi \rangle_i = \frac{d}{n^0}\sum_{j \neq i}\left[\frac{\phi_j - \phi_i'}{\left|\vec{r}_j - \vec{r}_i\right|^2}\left(\vec{r}_j - \vec{r}_i\right)w(r_{ij})\right] \tag{6}$$

where, the value of ϕ_i' is the minimum value among the neighboring particles within a range of radius r_e.

In the I-MPS, the particle number density n is used to instead of density ρ. The particle number density is calculated by the number and distance of surrounding particles and is regardless of the mass density of fluid. Thus, it is possible to set different particles with different mass densities. Since fresh concrete is assumed to be incompressible, the particle number density n is a constant, denoted by n^0 here. The n_i of particle i and its derivation with respect to time t are expressed as follows:

$$n_i = \sum_{j \neq i} w\left(\left|\vec{r}_j - \vec{r}_i\right|\right), \frac{dn_i}{dt} = \sum_{j \neq i}\frac{-r_e}{r_{ij}^3}\left(\vec{r}_{ij} \cdot \vec{u}_{ij}\right) \tag{7}$$

2.2. Slip layer treatment

It is generally considered that fresh concrete behaves as a non-Newtonian fluid with the yield stress that is a minimum stress for initiating irreversible flow. Also, fresh concrete is a complex fluid because it contains aggregates with a wide range of size. Dynamic segregation of aggregate is an additional factor that influences the pipe flow of fresh concrete. Segregation during concrete pumping involves the phenomena that aggregate particles tend to move towards the inner zone of pipe where the shear strain rate is lower. As a consequence, cement paste and a fraction of finer material move towards the pipe wall, forming a slip layer [8]. The pipe flow of concrete typically includes three layers or regions, as shown in Fig. 3: (i) slip layer or lubrication layer, (ii) shearing zone, (iii) plug flow zone. The total of the shearing layer and the plug flow layer is referred to as bulk concrete. Kaplan suggested that at a low pumping velocity, the concrete moves as a block in the pipe, with only a very thin slip layer near the pipe wall (often identified as plug flow). As the velocity increases, the pressure imposed on bulk concrete is sufficient to initiate the shear flow of part of bulk concrete (the applied shear stress is greater than the yield stress), accordingly generating a viscous flow in the concrete [1].

Depending on the scale of observation, either a slip layer or a slip velocity may be observed [34]. For a large scale of observation (macroscopic level), an apparent slip velocity can be measured, whereas, at a small scale of observation, a fine material layer, i.e., slip layer appears, in which the slip velocity evolves from zero at the wall to the apparent slip velocity at the boundary of the slip layer and the bulk concrete (see Fig. 4).

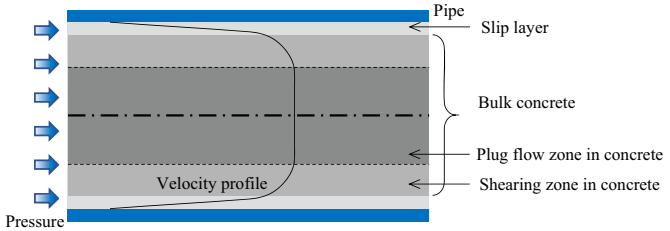

Fig. 3. Concrete flow in pipe.

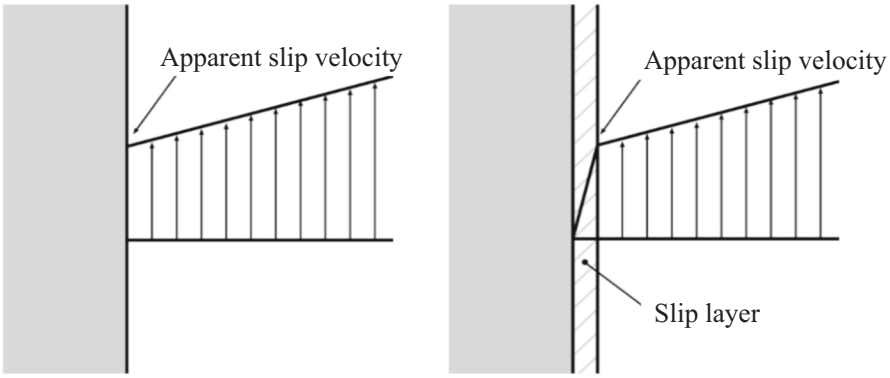

Fig. 4. Apparent slip velocity and slip layer: velocity in the fluid at the fluid –solid interface. Macroscopic scale (left) microscopic scale (right) [34].

Aleekseev [35] and Weber [36] first reported the existence of slip layer, and it was confirmed and investigated widely by the experiments and the numerical simulations [8,14,32]. The slip layer is highly sheared since it contains more liquid and fine particles and has a lower value of maximum aggregate size, accordingly with smaller yield stress and smaller viscosity than the bulk concrete [30]. The thickness of the slip layer has been widely debated and there is no consensus in the literature. Ngo et al. [38] found that the thickness of slip layer is proportional to the volume of the cement paste content, the water-cement ratio, and the dosage of superplasticizer in concrete, and it also decreases with the increase in the fraction of finer sand particles. The length and diameter of pipeline are also considered to be influencing factors of the slip layer's thickness. Ngo et al. [38] observed that the slip layer is between 1 mm to 9 mm thick, by visualizing the material flow in the rheometer. However, Choi et al. [6] found that the thickness of the slip layer is around 2 mm for the concretes, not depending on the volumetric flow rate, but varying with sand and gravel's initial volume fractions and pipe diameter. Le et al. [30] found by the PIV velocity measuring technique that the thickness of slip layer is not a constant in location and time, varying from 0 to 3 mm. Jo et al. [37] proposed that the slip layer ranges from about 1 mm to 5 mm thick, depending on the particle concentrations of cement, sand and gravel, as well as the pipe size, based on the numerical analysis of shear-induced particle migration. For special types of concrete, e.g. ultra-high performance concrete (UHPC), the slip layer is not formed by the shear-induced particle migration [8].

Several kinds of tribometer have been developed to measure the rheological properties (viscous constant and yield stress) of slip layer of fresh concrete [9,38–40]. Although the tribometers are different in structure and size, their fundamental principle is identical: a smooth cylinder is rotated in a container filled with fresh concrete sample to form a slip layer. Since no information on the thickness of slip layer is available [8], it is impossible to obtain the viscosity of slip layer using the rotational velocity-torque to shear rate-stress transformation, only getting the viscous constant (Pa·s/m) of slip layer that is a viscosity (Pa·s)-to-thickness (m) ratio. When measuring the rheological properties of the slip layer, it is desirable that only slip layer is sheared in tribometer. However, other two flow situations may be observed in tribometer for fresh concretes with different fluidity: i) Both slip layer and bulk concrete are completely sheared; ii) slip layer is sheared while concrete is partially sheared. In these two situations, a correction must be made to the measured rotational velocity for removing the effect of the sheared concrete. That is to say, accurate measurement of rheological properties of slip layer is still an issue.

Since the slip layer and the bulk concrete have different rheological properties and different particle sizes, in the numerical analysis of concrete pumping, the computed concrete should be divided into two zones: slip layer and bulk concrete. When the rheological properties of slip layer is measured by tribometer or other devices, an assumption about the thickness of the slip layer is required, which is not easy to clearly define [11]. Also, though in this study we proposed the DPMP model, as explained in Section 2.3, to make that the particles with different sizes can be used in the I-MPS simulation, numerically expressing the tiny particles in the slip layer by very small elementary particle will result in a long calculating time because numerous elementary particles are required in the simulation.

In this study we do not aim at clarifying the formation mechanism of slip layer. For avoiding an assumption of slip layer's thickness and reducing the number of discrete particles in the numerical simulation of pipe flow, apparent slip velocity is used to represent the flow of slip layer from macroscopic viewpoint. The flow velocity of slip layer at inside pipe wall surface to be zero [6], and the slip layer's thickness is ignored, i.e. the slip layer is not included as a part of fresh concrete. However, the effect of disregarding slip layer's thickness on the flow simulation was discussed in the latter part of this paper. Also, the shear resistance caused by the deformation of slip layer is called slip resistance here.

Le et al. [30], Suzuki et al. [16], and Feys et al. [4] focused on the macro effect of slip layer, and used a tribological behavior model to calculate the slip resistance. In the tribological behavior model, the slip resistance stress is a linear function of the slip velocity and has a slip yield stress, as follows:

$$\tau_L = \eta_L \cdot V_L + \tau_{L0} \tag{8}$$

where, τ_L is slip resistance stress, η_L is viscous constant of slip layer (Pa·s/m), τ_{L0} is slip yield stress of slip layer (Pa), V_L is apparent slip velocity of slip layer (m/s).

It should be noted that the slip yield stress is essentially different from the yield stress of the Bingham constants. It is the minimum stress for initiating the slip flow of slip layer, while the yield stress of fresh concrete is the minimum shear stress for initiating the shear flow.

As the thickness (δ) of slip layer is several millimeters, a smaller size, compared to the radius of pipe [6]. If disregarding this thickness, the average slip resistance stress of slip layer can be approximated as $\tau_L = RP/2L$. Therefore, the V_L in Eq. (8) can be calculated by Eq. (9). Since the pressure on the free surface is zero, the pressure gradient can be expressed by P/L.

$$V_L = \frac{RP/2L - \tau_{L0}}{\eta_L} \tag{9}$$

where, R is inner radius of pipe, L is concrete length, P is pressure.

The velocity profile of pipe flow is shown in Fig. 5. The total volumetric flow rate Q is formed by the volumetric flow rate Q_B induced by the shear deformation of bulk concrete, and the volumetric flow rate Q_L induced by the flow of slip layer. When considering the bulk concrete to be a Bingham fluid, the Q_B can be calculated according to the Buckingham-Reiner equation [3], as shown in the following.

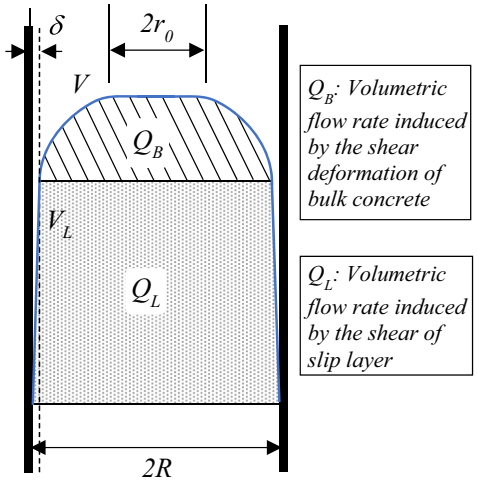

Fig. 5. Velocity profile of pipe flow considering slip layer.

$$Q_B = \frac{\pi(R-\delta)^4}{8\mu_b}\frac{P}{L}\left[1-\frac{4}{3}\left(\frac{r_0}{R-\delta}\right)+\frac{1}{3}\left(\frac{r_0}{R-\delta}\right)^4\right] \tag{10}$$

where, r_0 is radius of plug flow, which equals to $2\tau_b \cdot L/P$, and τ_b, μ_b are yield stress, and plastic viscosity of bulk concrete, respectively.

The Q_L can be obtained by:

$$Q_L = \pi R^2 \cdot V_L = \pi R^2 \frac{RP/2L - \tau_{L0}}{\eta_L} \tag{11}$$

Combining Eqs. (10) and (11), the relationship between the volumetric flow rate and pressure is obtained, as follows:

$$Q = \frac{\pi(R-\delta)^4}{8\mu_b}\frac{P}{L}\left[1-\frac{4}{3}\left(\frac{r_0}{R-\delta}\right)+\frac{1}{3}\left(\frac{r_0}{R-\delta}\right)^4\right]+\frac{\pi R^2}{\eta_L}\left(\frac{R}{2}\frac{P}{L}-\tau_{L0}\right) \tag{12}$$

However, when the thickness of slip layer is ignored, Eq. (12) can be simplified as:

$$Q \approx \frac{\pi R^4}{8\mu_b}\frac{P}{L}\left[1-\frac{4}{3}\left(\frac{r_0}{R}\right)+\frac{1}{3}\left(\frac{r_0}{R}\right)^4\right]+\frac{\pi R^2}{\eta_L}\left(\frac{R}{2}\frac{P}{L}-\tau_{L0}\right) \tag{13}$$

Usually, the volumetric flow rate Q_B of bulk concrete accounts a small percentage of total flow rate, and the thickness of slip layer is very small, this approximation does not cause a large error.

2.3. Constituent models of fresh concrete

Two types of constituent models were used to describe fresh concrete (see Fig. 6) [31]. In the single-phase & mono-particle (SPMP) model, as shown in Fig. 6 (a), fresh concrete is regarded as a single-phase homogeneous fluid represented by spherical discrete particles with same size and specific gravity. But in the double-phase & multi-particle (DPMP) model, as shown in Fig. 6 (b), fresh concrete is regarded as two-phase granular fluid of coarse aggregate (CA) and matrix mortar having different densities. CA particles have different sizes and random shapes, but matrix mortar phase is represented by spherical particles with same diameter.

In the I-MPS, if discrete particles have different sizes, the influencing area of each particle is different, and the interaction between the particles becomes asymmetrical. To avoid this problem, the Passively Moving Solid (PMS) model [41] was applied to calculate the movement of CA particles. CA particle is formed by several elementary particles, as shown in Fig. 7. The elementary particle is spherical and has the same size to mortar particle but its specific gravity is different from the mortar particle. The number of elementary particles forming a CA particle depends on the shape and size of the CA particle, and the size of the elementary particle. For easy visualization of simulation output, the CA particles with different shapes are simplified as circles with different

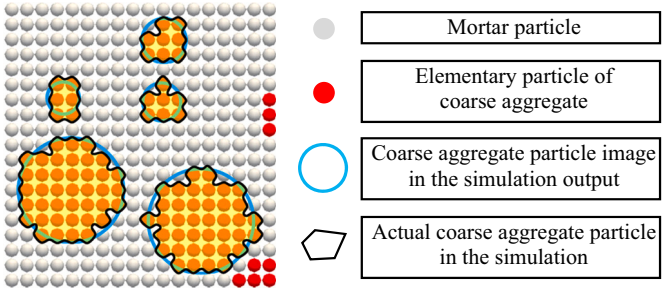

Fig. 7. Formation and shape of coarse aggregate particle in the DPMP model [31].

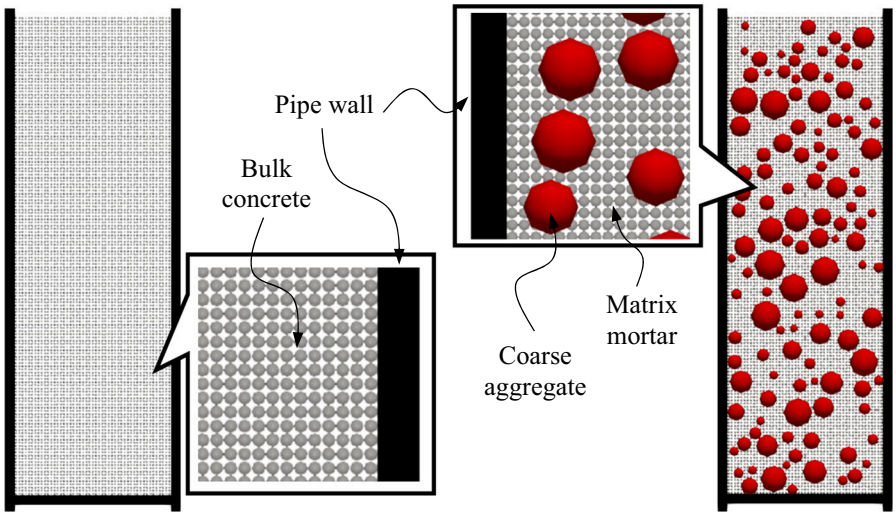

Fig. 6. Constituent models of fresh concrete [31].

diameters in 2D figuration, as shown in Figs. 6 (b), 14, 15, and 19.

According to the PMS model, the position of CA particle is determined by two steps (see Fig. 8). In the first step, the elementary particles move freely under its self-gravity and the interaction between the elementary particles. In the next step, each CA particle is treated as a rigid body, and the velocities and positions of element particles are revised on basis of the conservation of angular momentum to ensure that the elementary particles do not separate away and the shape of the CA particle is unchanged. Detailed description can be found in Ref. [27].

2.4. Rheological model of bulk concrete

Fresh concrete is a non-Newtonian fluid, and Bingham-type rheological model is generally used to describe the relationship between the shear stress τ and the shear strain rate $\dot{\gamma}$. For avoiding the numerical divergence occurring when $\tau \leqq \tau_b$, the following regularized Bingham model is generally used in place of the original Bingham model [23,42].

$$\tau = \mu_b \cdot \dot{\gamma} + \tau_b \cdot \left(1 - e^{-\beta\dot{\gamma}}\right) \tag{14}$$

where, τ_b is yield stress, μ_b is plastic viscosity. β is a parameter (=100, in this study) related to the transition between solid and fluid regimes, and the larger the β, the closer the regularized Bingham model is to the original Bingham model, but it is reported that the numerical solution is insensitive to β when $\beta > 10$ [43].

Thus, the dynamic viscosity μ used for numerical computation is represented by:

$$\mu = \mu_b + \tau_b \frac{1 - e^{-\beta\dot{\gamma}}}{\dot{\gamma}} \tag{15}$$

2.5. Interaction models between particles in fresh concrete

In the SPMP model, fresh concrete is regarded as one-phase fluid, all of the discrete spherical particles have the same density and size. The interactions of discrete particles are calculated by using the Bingham constants (μ_b, τ_b) of fresh concrete. According to Eq. (15), the dynamic viscosity of fresh concrete changes with the shear strain rate. The harmonic mean inter-particle viscosity, recommended by Shakibaeinia et al. [44], was adopted to improve the accuracy of numerical simulation, and the Laplacian in the viscosity Poisson equations and the pressure Poisson equations for calculating the interaction between the discrete particles are shown as follows:

$$\left\langle \frac{\mu}{\rho} \nabla^2 \vec{u} \right\rangle_{ij} = \frac{5-d}{n^0} \cdot \frac{2\mu_i \mu_j}{\mu_i + \mu_j} \cdot \frac{1}{\rho_C} \cdot \frac{\vec{u}_{ij} r_e}{r_{ij}^3} \tag{16}$$

$$\left\langle \frac{1}{\rho} \nabla^2 P \right\rangle_{ij}^{k+1} = \frac{5-d}{n^0} \cdot \frac{1}{\rho_C} \cdot \left(P_j^{k+1} - P_i^{k+1}\right) \cdot \frac{r_e}{\left|\vec{r}_j^{\,*} - \vec{r}_i^{\,*}\right|^3} \tag{17}$$

where, ρ_C is density of fresh concrete. μ_i and μ_j are dynamic viscosity of fresh concrete particles i and j for numerical simulation. Both of them are calculated according to the plastic viscosity of fresh concrete and the instantaneous shear strain rate.

The pressure gradient is calculated as following:

$$\left\langle \frac{1}{\rho} \nabla P \right\rangle_i = \frac{d}{n^0} \sum_{j \neq i} \left[\frac{2\left(P_j - P_{i,min}\right)}{\rho_C \left|\vec{r}_j^{\,*} - \vec{r}_i^{\,*}\right|^2} \left(\vec{r}_j^{\,*} - \vec{r}_i^{\,*}\right) w\left(r_{ij}^*\right) \right] \tag{18}$$

where, $P_{i,\min}$ is the minimum pressure among the neighboring particles.

On the other hand, in the DPMP model with matrix mortar particles and CA particles, there are three kinds of interaction between particles: (a) between mortar particles, (b) between CA particles, (c) between mortar particle and CA particle, as shown in Fig. 9. The interaction between two mortar particles is calculated by using the viscosity of matrix mortar. The interaction between two CA particles is calculated by using the rheological parameters of CA particle. When calculating the interaction between mortar particle and CA particle, the respective viscosity of two phases is used, as shown in Fig. 9 (c). Duan et al. [45] suggested to use arithmetic mean density to improve the stability of the numerical results. The viscous and pressure interaction between two particles can be calculated by the following multi-viscosity model and multi-density model, respectively.

$$\left\langle \frac{\mu}{\rho} \nabla^2 \vec{u} \right\rangle_{ij} = \frac{5-d}{n^0} \cdot \frac{2\mu_i \mu_j}{\mu_i + \mu_j} \cdot \frac{2}{\rho_i + \rho_j} \cdot \frac{\vec{u}_{ij} r_e}{r_{ij}^3} \tag{19}$$

$$\left\langle \frac{1}{\rho} \nabla^2 P \right\rangle_{ij}^{k+1} = \frac{5-d}{n^0} \cdot \frac{2}{\rho_i + \rho_j} \cdot \left(P_j^{k+1} - P_i^{k+1}\right) \cdot \frac{r_e}{\left|\vec{r}_j^{\,*} - \vec{r}_i^{\,*}\right|^3} \tag{20}$$

The pressure gradient in the DPMP model is divided into two terms for fresh concrete composed of two kinds of particles with different densities as follows [45]:

$$\left\langle \frac{1}{\rho} \nabla P \right\rangle_i = \frac{d}{n^0} \sum_{j \neq i} \left[\frac{2\left(P_j - P_i\right)}{\left(\rho_i + \rho_j\right) \left|\vec{r}_j^{\,*} - \vec{r}_i^{\,*}\right|^2} \left(\vec{r}_j^{\,*} - \vec{r}_i^{\,*}\right) w\left(r_{ij}^*\right) \right] + \frac{d}{n^0} \sum_{j \neq i} \left[\frac{\left(P_i - P'_{i,min}\right)}{\rho_i \left|\vec{r}_j^{\,*} - \vec{r}_i^{\,*}\right|^2} \left(\vec{r}_j^{\,*} - \vec{r}_i^{\,*}\right) w\left(r_{ij}^*\right) \right] \tag{21}$$

where, $P'_{i,\min}$ is the minimum pressure among the same type of neighboring particles of particle i.

The Bingham constants of bulk concrete (μ_b, τ_b) and matrix mortar (μ_M, τ_M) can be measured directly by a rheometer. However, there is currently no method to determine the rheological parameters (μ_{CA}, τ_{CA}) of CA particles. We proposed an method to estimate the μ_{CA} and the τ_{CA} by using the Bingham constants of matrix mortar and fresh concrete, and the volume fraction and the maximum packing volume fraction of CA [31].

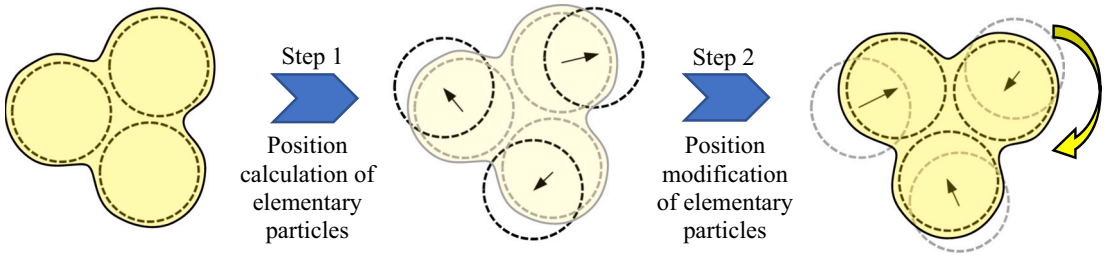

Fig. 8. Position calculation and modification of CA particle [31].

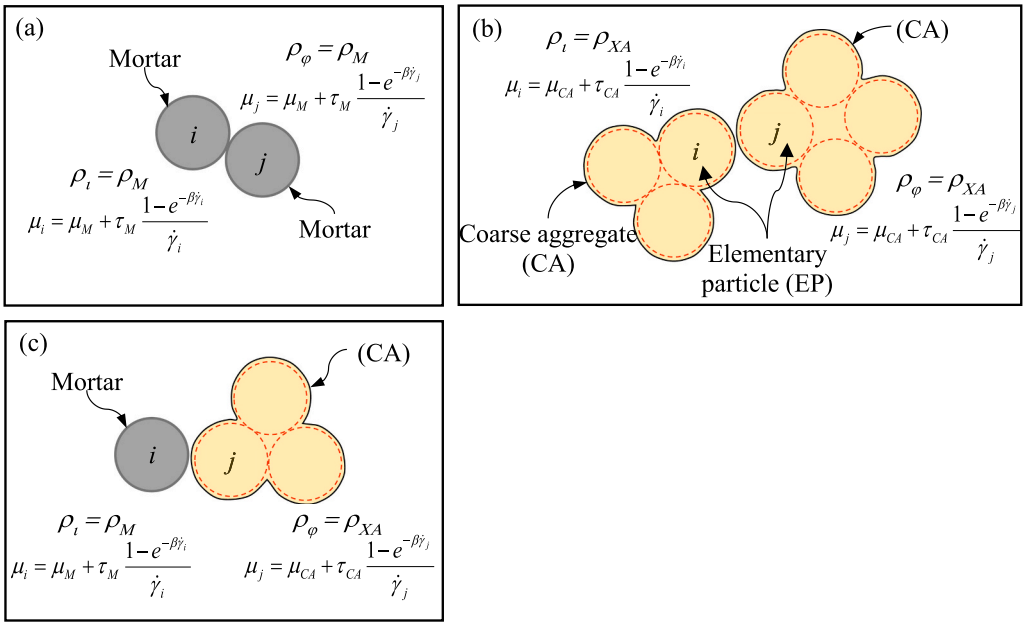

Fig. 9. Three types of particle interaction models in fresh concrete.

3. Numerical simulation

3.1. Concrete mixtures

In our simulation, three series of concrete were used, of which mix proportions are presented in Table 1. Ordinary Portland cement with the Blaine fineness of 3410 cm^2/g and the density of 3150 kg/m^3 was used in these concretes. The fine aggregate had the particle size of 0–5 mm and the surface dry density of 2620 kg/m^3, and its water absorption capacity was 2.45% and fineness modulus was 2.83. CA was gravel with the size 5–20 mm and its surface dry density was 2630 kg/m^3. Water absorption capacity of gravels was 1.15% and its fineness modulus was 6.72. A polycarboxylate ether compound-based superplasticizer was added. The viscosity modifying agent used is mainly composed of cellulose-based compound. It is found in Ref. [16] that the slump values of the concretes were 13 cm, 18 cm, and 22 cm, respectively, and the bulk densities of the concretes were 2354 kg/m^3, 2345 kg/m^3, and 2338 kg/m^3, respectively.

3.2. Rheological properties

The Bingham constants of the fresh concretes are shown in Table 2. [16]. These constants were measured by a BML rheometer in Ref. [16]. The radius of the inner cylinder of the BML rheometer was 150 mm, the height was 200 mm, and the radius of the outer cylinder was 200 mm.

In Ref. [16], a series of pipe flow experiments were conducted for different volumetric flow rates to calculate the parameters η_L, τ_{L0} of the slip resistance model shown in Eq. (8). The pumping device used in the experiments is shown in Fig. 10. A seamless stainless-steel mobile pipe had an inner radius of 5 cm and a length of 2 m. The mobile pipe was connected to a docking hose of pump. The joint was an acrylic sleeve with an inner diameter of 1 mm larger than the diameter of outer mobile pipe, so that the mobile pipe can move horizontally under the concrete's slip resistance when fresh concrete was pumped. The slip resistance force of concrete pumping was detected by a proving ring. The pressure in the pipe was measured by a diaphragm type pressure sensor, which was located at 15 cm far from the inlet of the mobile pipe. Several volumetric flow rates in the pipe were measured, which corresponded to different pressures. Based on the values of volumetric flow rate and the pressures provided by Ref. [16], we calculated the η_L and the τ_{L0} of slip layer with different thickness by using Eq. (12). The calculated results are shown in Table 3. It can be seen that no matter if the thickness of slip layer was considered and no matter what thickness was used, the calculated result of τ_{L0} had no difference, and the η_L decreased slightly with the increase in the thickness of slip layer. Hence, in the following simulations, the η_L and the τ_{L0} of 0 mm thickness of slip layer were used.

Table 2
Bingham constants of fresh concretes [16].

Series	No.1	No.2	No.3
μ_b (Pa·s)	397	305	297
τ_b (Pa)	190	181	149

Notes: μ_b is plastic viscosity, τ_b is yield stress.

3.3. Configuration of numerical simulations

The smaller the elementary particle is, the closer the CA particle, formed from the elementary particle, will be to the actual size and shape of the CA particle in the I-MPS simulation. However, using small elementary particle will have to use so many elementary particles to

Table 1
Mix proportions of concrete mixture [16].

Series	Cement (kg/m^3)	Sand (kg/m^3)	Gravel (kg/m^3)	Water (kg/m^3)	SP (%)	VMA (%)	Bulk density (kg/m^3)	Slump (cm)
No.1	323	912	946	171	0.808	0.646	2354	13
No.2	338	890	936	179	0.845	0.676	2345	18
No.3	360	872	913	191	0.900	0.720	2338	22

Notes: SP is superplasticizer, VMA is viscosity modifying agent.

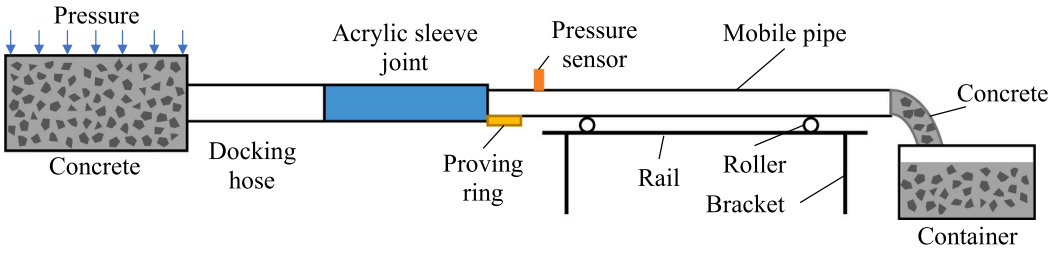

Fig. 10. Slip resistance measurement device for fresh concrete.

Table 3
Rheological parameters of slip resistance equation.

Series	Rheological parameters	Thickness of slip layer (mm)			
		0*	2	4	6
No.1	η_L (Pa·s/m)	893	889	885	882
	τ_{L0} (Pa)	251	251	251	251
No.2	η_L (Pa·s/m)	844	839	834	831
	τ_{L0} (Pa)	239	239	239	239
No.3	η_L (Pa·s/m)	922	914	908	902
	τ_{L0} (Pa)	204	204	204	204

Notes: η_L is viscous constant of slip layer, τ_{L0} is slip yield stress of slip layer, * the parameters of 0 mm thickness are referred to Ref. [16], but for other thicknesses, the parameters were calculated by Eq. (12).

form CA particles that long calculation time is needed unless parallel computation is conducted. For performing the pipe flow simulation in personal computer and cutting down the calculation time, two-dimensional calculation was adopted in this study, so that the particles were circular, not spherical. And the selection of diameter of elementary particle requires a balance between calculation time and calculation accuracy.

In 3D (three-dimension) vertical pipe flow, the pumping pressure can be expressed theoretically by:

$$P_{3D} = \rho g L + \frac{\tau_L \cdot 2\pi R \cdot L}{\pi R^2} = \rho g L + \frac{2\tau_L \cdot L}{R} \tag{22}$$

However, in case of two-dimension (2D) model, the pipe wall is simplified into two lines from a circumferential surface in 3D, as illustrated in Fig. 11, thus the pumping pressure should be calculated by:

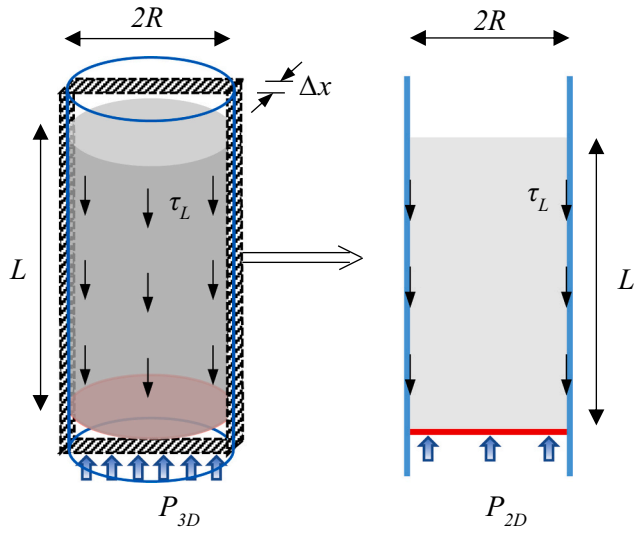

Fig. 11. Pressure analysis in 3D and 2D models.

$$P_{2D} = \rho g L + \lim_{\Delta x \to 0} \frac{\tau_L \cdot 2L \cdot \Delta x}{2R \cdot \Delta x} = \rho g L + \frac{\tau_L \cdot L}{R} \tag{23}$$

It can be found that the pressure loss caused by the slip resistance in 2D is half of that in 3D. By combining Eqs. (8), (12), and (23), the *P-Q* relationship in 2D vertical pipe flow can be obtained as:

$$Q = \frac{\pi (R-\delta)^4}{4\mu_b} \cdot \frac{(P_{2D} - \rho g L)}{L} \left[1 - \frac{4}{3}\left(\frac{r_0}{R-\delta}\right) + \frac{1}{3}\left(\frac{r_0}{R-\delta}\right)^4\right] + \frac{\pi R^2}{\eta_L}\left[R \cdot \frac{(P_{2D} - \rho g L)}{L} - \tau_{L0}\right] \tag{24}$$

When the thickness of slip layer is disregarded, Eq. (24) can be simplified as:

$$Q \approx \frac{\pi R^4}{4\mu_b} \cdot \frac{(P_{2D} - \rho g L)}{L} \left[1 - \frac{4}{3}\left(\frac{r_0}{R}\right) + \frac{1}{3}\left(\frac{r_0}{R}\right)^4\right] + \frac{\pi R^2}{\eta_L}\left[R \cdot \frac{(P_{2D} - \rho g L)}{L} - \tau_{L0}\right] \tag{25}$$

The V_L can be calculated by:

$$V_L = \frac{R(P_{2D} - \rho g L)/L - \tau_{L0}}{\eta_L} \tag{26}$$

In the flow simulation using any of particle methods, the more the particles, the slower the calculation. Using large particles can reduce the number of particles, but may harm the simulation precision. Thus, in this study, we firstly did the resolution convergence study to discuss suitable particle size, and investigated whether disregarding the thickness of slip layer greatly affects the simulation result. These investigations were conducted through 2D vertical pipe flow simulation of series No.1, using the SPMP model. The length of concrete was 300 mm, and the inner diameter of vertical pipe was 100 mm. In the simulation, the volumetric flow rate of concrete was first set up, the inlet flow velocity was then calculated by dividing the volumetric flow rate by the pipe cross-sectional area. Besides the slip resistance of slip layer described by Eq. (8), the Dirichlet boundary condition was considered. The pressure on the free surface was set to be zero, and the boundary particles should satisfy the same pressure calculation equation (see Eq. (4)), as the discrete particles. The piston was moved in the vertical pipe at the inlet flow velocity. The time step was set as 0.0005 s, and the calculation time was 5 s.

When the volumetric flow rate Q is 1500 cm^3/s, the 2D pumping pressure P_{2D} and the apparent slip velocity V_L were 9.40 kPa, and 18.6 cm/s, respectively, according to Eqs. (25) and (26).

The resolution convergence study was conducted by using different particle-center distances, i.e., the particle diameter, which were 20 mm, 10 mm, 5 mm, 3 mm, and 2 mm, respectively, and the thickness of slip layer was ignored. A comparison between the theoretical pressure (9.40 kPa) and the calculated pressures of flow simulations is shown in Fig. 12. It is shown that the smaller the fluid particle, the closer the calculated pressure is to the theoretical value, but the simulation results are almost independent of the particle diameter when it is less than 5 mm. Hence, in the following simulations, the diameters were set as 2 mm for the fluid particles in the SPMP model, and for the elementary particles in the DPMP model.

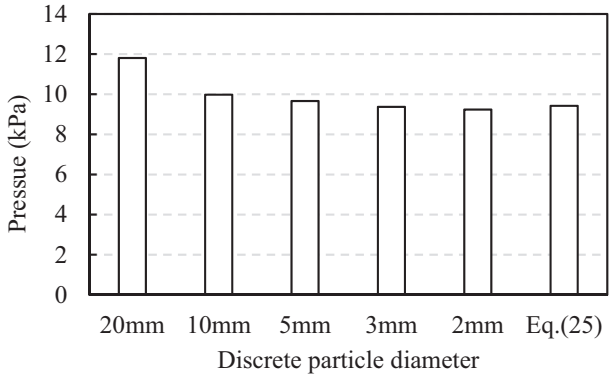

Fig. 12. Pumping pressure under 1500 cm^3/s of flow rate, calculated by using different diameters of fluid particle.

Since we used a macroscopic approach to treat the slip layer, the thickness of slip layer is disregarded in the flow simulation, i.e., the radius of bulk concrete is equal to the inner radius of the vertical pipe. However, for clarifying the effect of disregarding the thickness of slip layer, we assumed three thicknesses of slip layer and calculated the rheological constants η_L and τ_{L0} by Eq. (12), as shown in Table 3. The radius of bulk concrete is a difference between the inner radius of the pipe and the thickness of slip layer. Fig. 13 shows the effect of bulk concrete's radius on the calculated pressures of Concrete No.1's vertical pipe flow. Though considering the thickness of slip layer to reduce the bulk concrete's radius yielded different calculated pressures, they were not greatly different from the theoretical value, even the thickness was set to be 0 mm (the radius of bulk concrete was 50 mm). It is also found with the increase of the thickness, the calculated pressure slightly increased. This is because the increase of the thickness results in a decrease of bulk concrete volume, accordingly a high pressure is required for the same volumetric flow rate. In summary, disregarding the thickness of slip layer has no great effect on the simulation result. As explained in Section 2.2, the volumetric flow rate Q_B of bulk concrete accounts a small percentage of the total flow rate Q, the small change of bulk concrete in size does not result in a great change of pressure.

After the discussion above, vertical pipe flow simulations were conducted for the three concretes using the I-MPS. Like as the investigations on the reasonable particle diameter and the effect of slip layer's thickness, the concretes length was 300 mm, and the inner diameter of vertical pipe was 100 mm. When using the SPMP model, three series of fresh concrete were represented respectively by 7350 round discrete particles with 2 mm diameter, and all the discrete particles had the same density to the concrete. However, in the DPMP model, the difference of density between matrix mortar and CA was considered for analyzing the dynamic segregation of CA. In the Concrete No.1 ~ No.3, we used 4666, 4733, and 4797 mortar particles with 2 mm diameter, respectively, and the number of CA particles was 119, 118, and 113, respectively, which were randomly distributed in the matrix mortar. The CA particles were formed by the elementary particles of 2 mm diameter. The same CA was used to mix three concretes. The volume fractions of CA particles in the range of 5–10 mm, 10–15 mm and 15–20 mm were set to be 30%, 40%, and 30%, respectively, for making the fineness modulus (F.M.) of simulated CA to be consistent with the actually measured value (= 6.72). The detail configuration information of particles was shown in Table 4. Moreover, the SPMP model and the DPMP model used the same parameters of slip layer, and the same Bingham constants of bulk concrete for a given concrete.

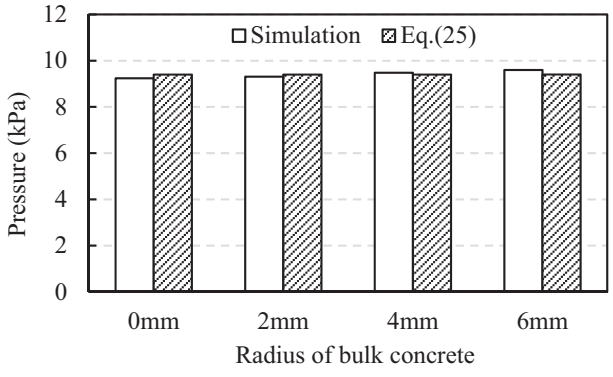

Fig. 13. Pumping pressure under 1500 cm^3/s of flow rate, considering different thicknesses of slip layer.

4. Numerical results and discussion

Using the I-MPS and the two constituent models of fresh concrete, the upward flow of the three concretes in the vertical pipe was simulated for different volumetric flow rates (Q). The thickness of the slip layer was not considered, i.e., the diameter of bulk concrete was equal to the inner diameter of pipe. The rheological parameters shown in Tables 2 and 3 were used for characterizing the shear flow of concrete and the slip flow of slip layer, respectively. For a certain volumetric flow rate Q, the corresponding moving speed of the piston was firstly calculated by $Q/\pi R^2$. Then, upward pipe flow was simulated to get 2D pumping pressure and velocity profiles by driving the lowest particles that contact the piston move at the speed of the piston. For a comparison with the numerical results, theoretical two-dimensional P-Q relationships were also obtained by using Eq. (25).

As an example of numerical results, Figs. 14 and 15 show the pressure distribution and the velocity profiles in the Concrete No.1 that was pumped at a flow rate of 1500 cm^3/s. It should be noted that this velocity profiles refer to bulk concrete (= whole concrete here due to no thickness of slip layer), do not include the slip velocity of slip layer. Present program outputs round shape images for the CA particles, but in the actual simulation, the CA particles were formed by the elementary particles, thus have random shapes, as explained in Fig. 7. From Fig. 14, it can be found that the pressure distributions obtained by the SPMP model and the DPMP model are almost the same, and the pressure gradually decreases from the bottom to the upper of concrete. From Fig. 15, we can see that a plug flow zone is formed in the center of the pipe. The flow velocity of concrete near the pipe wall is slower than that around the center axis because of the wall effect. This phenomenon is more obvious in the DPMP model, because the CA particles near the pipe wall obstruct the shear flow of the matrix mortar. The flow velocity of the front concrete is almost the same as the end concrete. The simulated pressure (P)-flow rate (Q) relationships, velocity profiles in different zones, as well as dynamic segregation of CA will be discussed in the following.

4.1. Pumping pressure-flow rate relationship

The pressure (P)-volumetric flow rate (Q) relationships of three series of fresh concrete are shown in Fig. 16. For any of the concretes, no matter which constituent model was used, the numerically P-Q relationship are well coincident with the theoretically one. Therefore, it is possible to use the I-MPS to predict pumping pressure of concrete. When only the pressure is needed to calculate, the SPMP model is convenient, since it is not necessary to form CA particles with elementary particles and modify the positions of the elementary particles at each step.

Fig. 17 shows a detailed comparison between the numerically calculated pressures and the theoretically calculated pressures under the flow rate Q = 1500 cm^3/s. All the numerical pressures are consistent with the theoretical results by the errors of less than 3%. The error may be caused by the influence of ignoring the thickness of slip layer. The errors when using the DPMP model are slightly lower than those of using the SPMP model. Considering the size distribution and the shape of CA would be benefit to the calculation precision of pumping pressure.

Table 4
Configuration information of particles.

Series of concrete	Single-phase & mono-particle model			Double-phase & multi-particle model					
	Discrete particle			Mortar particle			Coarse aggregate particle		
	Density (kg/m^3)	Shape, diameter	Number	Density (kg/m^3)	Shape, diameter	Number	Density (kg/m^3)	Shape, size	Number
No.1	2354	Round, 2 mm	7350	2190	Round, 2 mm	4666	2630	Random	119
No.2	2345			2187		4733		5–10 mm, 30%	118
No.3	2338			2182		4797		10–15 mm, 40%	113
								15–20 mm, 30%	

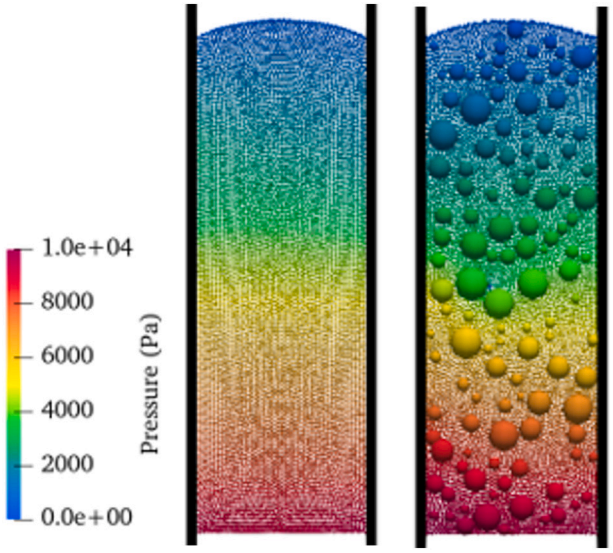

Fig. 14. Pressure distribution in Concrete No.1 at a flow rate $Q = 1500$ cm^3/s ($t = 5$ s)
Left: SPMP model; Right: DPMP model.

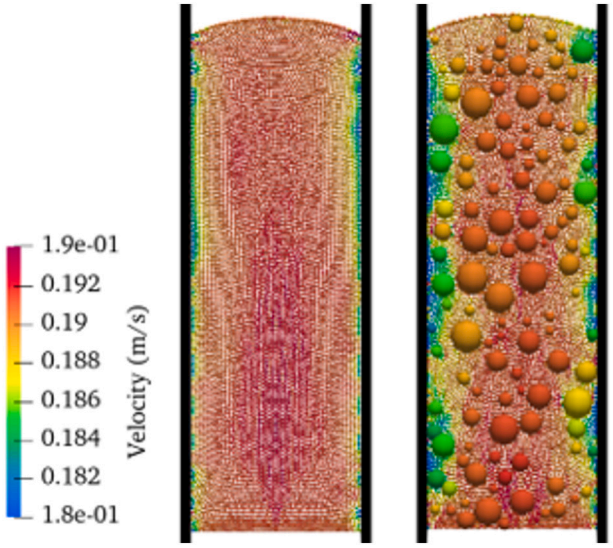

Fig. 15. Velocity profile in Concrete No.1 at a flow rate Q = 1500 cm^3/s ($t = 5$ s)
Left: SPMP model; Right: DPMP model.

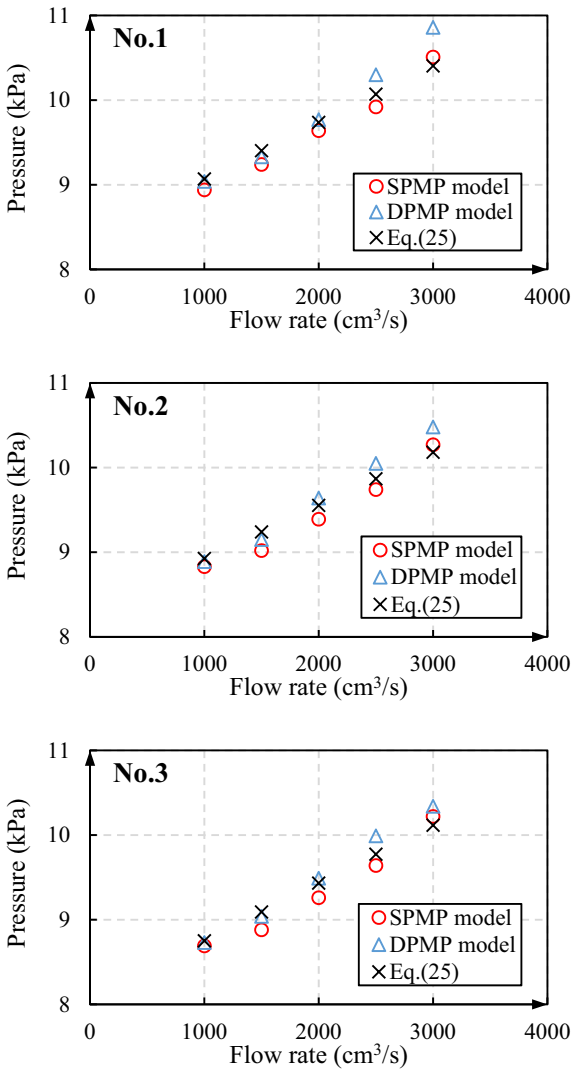

Fig. 16. Numerical and theoretical pressures under different flow rates for Concretes No.1 ~ No.3.

4.2. Velocity profile

During the simulation, the flow velocities from the pipe wall to the center axis were recorded for heights of 24 cm, 15 cm, and 6 cm from the piston at the bottom of concrete. The recorded velocity profiles at the three heights represent the flow characteristics of the concrete in the upper, middle and lower zones. Taking the Concrete No.1 as an example, Fig. 18 (a) and (b) show the velocity profiles calculated by using the SPMP model, and the DPMP model, respectively. Detailed variations of flow velocity from the pipe wall are shown in Fig. 18 (c) and (d). The characteristics of velocity profiles agree with the theoretical model of pipe flow shown in Fig. 5. It can be found that the velocity profiles of the

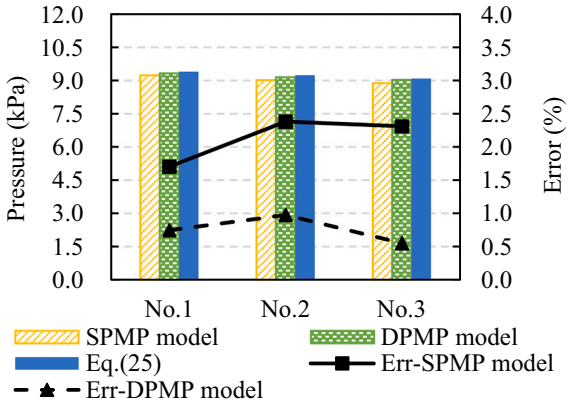

Fig. 17. Comparison of numerical and theoretical pressures.

concrete at different heights are almost the same. The shear rate (tangent slope of the velocity curve) of the concrete close to the pipe wall is very large. The farther the concrete is from the pipe wall, the lower the shear rate. For the SPMP model, the concrete in the central zone of about 1.0 cm radius, the flow velocity is almost uniform, showing a plug flow. However, for the DPMP model, the concrete in the central zone of about 2.0 cm radius shows a plug flow. That is to say, if the size, shape and density of CA are considered in the constituent model of concrete as its reality as possible, central zone of non-shear deformation will be enlarged due to a larger interaction between particles. Numerically calculated apparent slip velocities at the interface of pipe wall and concrete are 18.6 cm/s, and 18.4 cm/s, respectively, for the SPMP model and the DPMP model, which are well consistent with the theoretically calculated results (18.6 cm/s). Hence, both the proposed constituent models can be used to simulate the pipe flow of fresh concrete. However, as explained in the following, only the DPMP model would provide the dynamic segregation information of CA.

4.3. Migration of coarse aggregates

The positions of several CA particles in bulk concrete were noticed at different time points, as shown in Fig. 19. The blue color particles gradually came close, which were the CA particles in the end of the vertical pipe flow, and the CA particle in contact with the pipe wall moved downward due to the boundary resistance. The green color particles, locating in the central of the concrete, remained almost unchanged relative positions because of the plug flow. The orange color particles in the upper of the concrete changed in their relative positions due to the velocity difference between the inner and outer layers of the concrete.

Although the particles in different positions of the bulk concrete have different velocities, as shown in Fig. 15, the shear deformation of bulk concrete is not as large as that of the slip layer. Moreover, the time of flow simulation was only 5 s, the deformation of the bulk concrete was not very intensive. Therefore, the migration of CA particles in Fig. 19 was not obvious. To discuss the migration of CA particles in detail, as shown in Fig. 20, the concrete was divided into two portions in the radius direction (inner and outer portions), and in the flow direction (upper and lower portions), respectively, for investigating the variation of the distribution of CA particles with the vertical pipe flow. The volume fraction (φ) of the CA particles in each portion was counted, and the variations of the φ with the elapsed time are shown in Fig. 21. Fig. 21 (a) shows the variations of the φ along the radius direction. It was observed that the CA particles migrated towards the inside of bulk concrete. With the increase of flow time, the φ of the inner portion increased, but the φ of the outer portion decreased. This result well agrees with the well-known knowledge that large particles move towards the inner of concrete where the shear rate is lower [6,9]. Concrete No.1 had the lowest slump, compared to other two concretes, and the variation rate of the φ along the radial direction is the smallest. This means that the formation of the slip layer is slow for the fresh concrete with low fluidity. It was also noticed that this migration movement along the radius direction did not continue after 2 s. This is because as the volume fraction of CA particles increases, the obstacle to inward migration increases, and

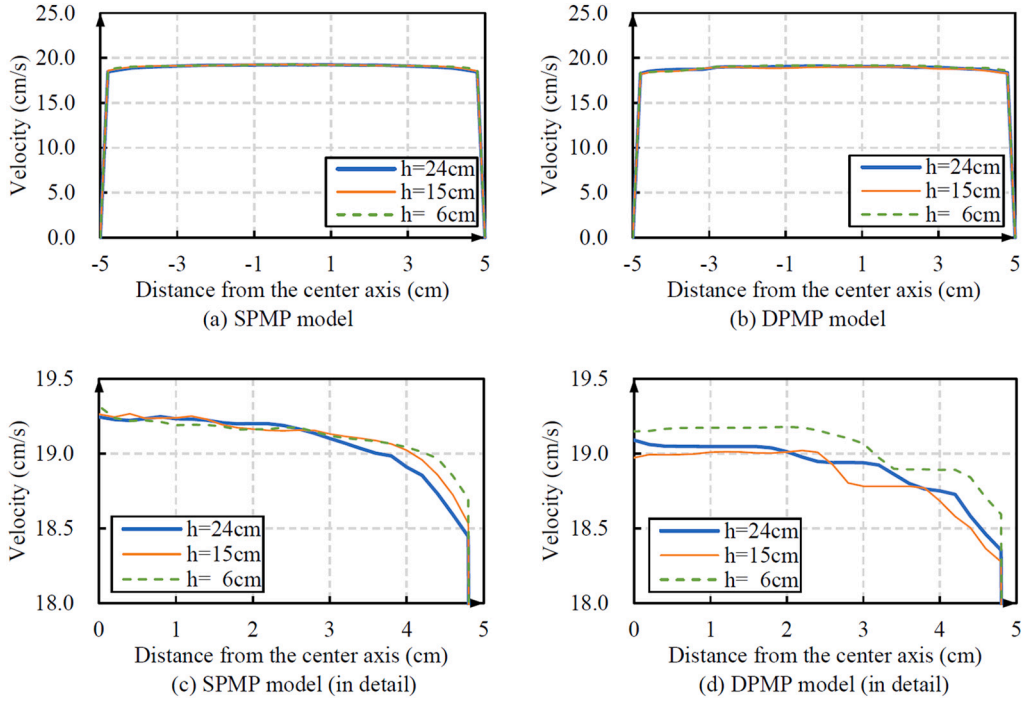

Fig. 18. Velocity profile in the pipe at different height h (Concrete No.1).

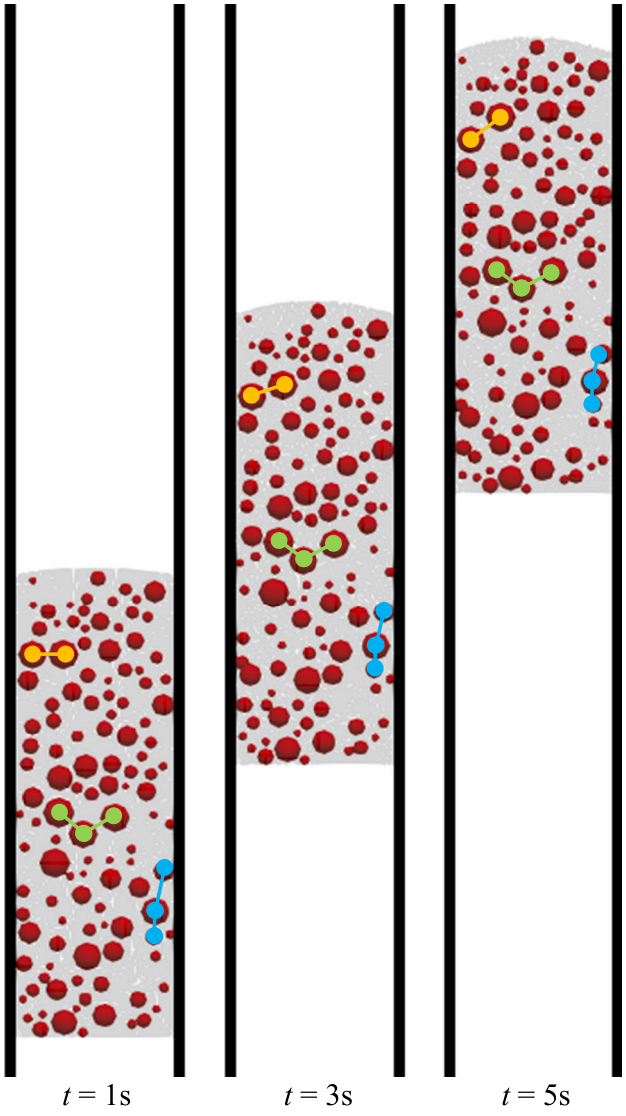

Fig. 19. Migration of coarse aggregates during pipe flow.

finally dynamic equilibrium is reached. Hence, This I-MPS simulation is possible to simulate the segregation behavior of fresh concrete during pipe flow.

The variations of the φ along the flow direction are shown in Fig. 21 (b). It is considered that the CA particles, under the action of viscosity and inertia, resist the impact of gravity and move ahead of the surrounding mortar [10], so that the φ in the front concrete is larger than that of the lower portion. Also, if concrete has lower viscosity, its CA is easier to segregate. This well-known fact can be found from Fig. 21 (b). Concrete No.2 and No.3 had lower viscosity (305 Pa·s, and 297 Pa·s, respectively) than Concrete No.1 (397 Pa·s), the variations of the φ of these two concretes were larger along the flow direction than Concrete No.1.

Hence, using the I-MPS and the DPMP model can not only predict the pressure and velocity profile of pipe flow, but also would be able to simulate the segregation behavior of CA. Detail numerical investigation on the formation of slip layer caused by shear-induced segregation and the influencing factors of dynamic segregation of pumped concrete will be reported in other papers.

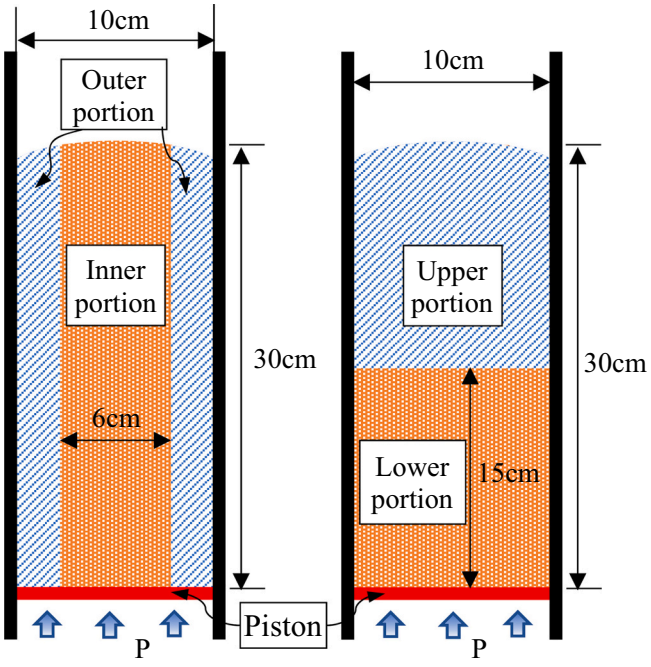

Fig. 20. Zoning of concrete for segregation analysis.

5. Summary

In this study, a new numerical approach, based on the I-MPS with complete implicit algorithm and the DPMP model, was developed for simulating the flow and segregation behaviors of fresh concrete in pipes. As a particle method, MPS is possible to simulate the segregation of behavior of aggregate particles that cannot be described by the CFD method, and MPS has the ability to avoid the compression of fluid particles under high pressure, which generally concurs in traditional SPH simulation, so as to be applicable to concrete pumping. Moreover, the complete implicit algorithm in the I-MPS can improve the calculating accuracy and shorten the calculating time of the general MPS. These advantages of the I-MPS make it more suitable for pumping flow simulation of fresh concrete than CFD, traditional SPH, and MPS.

The slip layer near the inside wall of pipe affects the pumpability of fresh concrete. However, the compositions and the thickness of the slip layer are not easy to be clearly defined. The tribological behavior model was adopted in our numerical approach to describe the slip resistance stress of the slip layer, which describes the flow of the slip layer by apparent slip velocity. This macroscopic approach solved the problems of unknown thickness and compositions of the slip layer.

Two types of constituent models were used to describe fresh concrete, called the single-phase & mono-particle (SPMP) model and the double-phase & multi-particle (DPMP) model. In the SPMP model, fresh concrete is regarded as a homogeneous fluid represented by the same spherical particles. But in the DPMP model, fresh concrete is regarded as a two-phase granular fluid of matrix mortar and coarse aggregate (CA) having different densities. Matrix mortar phase is represented by the same spherical particles. Spherical elementary particles are employed to form CA particles to permit them to have different sizes and random shapes. The elementary particles and the mortar particles have the same diameter but different densities. The macroscopic treatment of the slip layer avoided using numerous tiny elementary particles to represent the slip layer and the mortar and CA particles, thus greatly raise the calculation efficiency when using the DPMP model.

The numerical approach combined with any of the two constituent models is able to predict the pumping pressure of the pipe flow of fresh concrete, provided the rheological properties of fresh concrete can be expressed by the Bingham model. The numerical results of the pumping

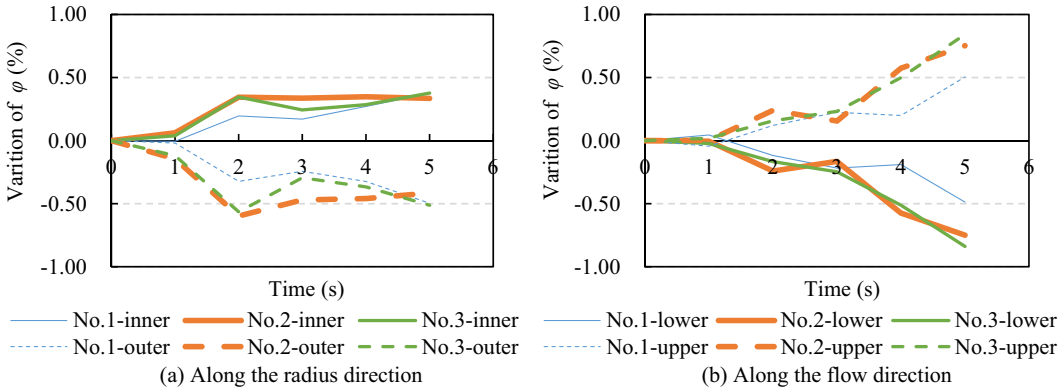

Fig. 21. Variations of volume fraction φ of coarse aggregate with pipe flow time.

pressure are consistent with the theoretical results obtained by the revised Buckingham-Reiner equation considering the flow of the slip layer. And when using the DPMP model, the dynamic segregation of coarse aggregate particles would be also simulated. Thus, this numerical approach has the potential to investigate numerically the formation of slip layer when using high-speed computers or parallel computing, and to discuss the influencing factors of the flow and aggregate segregation of pumped concrete.

CRediT authorship contribution statement

Zhisong Xu: Investigation, Software, Data Curation, Visualization, Writing-Original draft preparation.

Zhuguo Li: Conceptualization, Methodology, Visualization, Writing-Reviewing and Editing.

Fei Jiang: Software.

Declaration of competing interest

The authors declare that they have no known competing financial interests or personal relationships that could have appeared to influence the work reported in this paper.

References

[1] M. Jolin, D. Burns, B. Bissonnette, F. Gagnon, L.-S. Bolduc, B. Bissonnette, Understanding the pumpability of concrete, in: Shotcrete Undergr. Support XI, 2009.
[2] H. Kwon, C.K. Park, J.H. Jeong, S.D. Jo, S.H. Lee, Prediction of concrete pumping: part II — analytical prediction and experimental verification, ACI Mater. J. 110 (2013) 657–668.
[3] E. Buckingham, On plastic flow through capillary tubes, Proc. Am. Soc. Test. Mater. (1921) 1154–1156.
[4] D. Feys, G. De Schutter, R. Verhoeven, Parameters influencing pressure during pumping of self-compacting concrete, Mater. Struct. Constr. 46 (2013) 533–555.
[5] D.T. Kaplan, F. De Larard, Sedran, Design of concrete pumping circuit, ACI Mater. J. 102 (2005) 110–117.
[6] M. Choi, N. Roussel, Y. Kim, J. Kim, Lubrication layer properties during concrete pumping, Cem. Concr. Res. 45 (2013) 69–78.
[7] V. Mechtcherine, V.N. Nerella, K. Kasten, Testing pumpability of concrete using Sliding Pipe Rheometer, Constr. Build. Mater. 53 (2014) 312–323.
[8] G. De Schutter, D. Feys, Pumping of fresh concrete: insights and challenges, RILEM Tech. Lett. 1 (2016) 76.
[9] E. Secrieru, J. Khodor, C. Schröfl, V. Mechtcherine, Formation of lubricating layer and flow type during pumping of cement-based materials, Constr. Build. Mater. 178 (2018) 507–517.
[10] M. Choi, C.F. Ferraris, N.S. Martys, V.K. Bui, H.R.T. Hamilton, D. Lootens, Research needs to advance concrete pumping technology, Gaithersburg, MD, 2015.
[11] M. Choi, C.F. Ferraris, N.S. Martys, D. Lootens, V.K. Bui, H.R.T. Hamilton, Metrology deeds for predicting concrete pumpability, Adv. Mater. Sci. Eng. 2015 (2015) 1–10.
[12] D. Feys, G.De Schutter, R. Verhoeven, K.H. Khayat, Similarities and differences of pumping conventional and self-compacting concrete, in: RILEM Bookseries, 2010.
[13] E. Secrieru, W. Mohamed, S. Fataei, V. Mechtcherine, Assessment and prediction of concrete flow and pumping pressure in pipeline, Cem. Concr. Compos. 107 (2020), 103495.
[14] J.S. Kim, S.H. Kwon, K.P. Jang, M.S. Choi, Concrete pumping prediction considering different measurement of the rheological properties, Constr. Build. Mater. 171 (2018) 493–503.
[15] D. Feys, K.H. Khayat, A. Perez-Schell, R. Khatib, Prediction of pumping pressure by means of new tribometer for highly-workable concrete, Cem. Concr. Compos. 57 (2015) 102–115.
[16] K. Suzuki, S. Koshikawa, Y. Itoh, Studies on pipe flow of concrete, Concr. Res. Technol. 15 (2004) 47–57.
[17] D. Kaplan, Pompage des bétons, Ecole Nationale des Ponts et Chaussées, 1999.
[18] M.S. Choi, Y.J. Kim, S.H. Kwon, Prediction on pipe flow of pumped concrete based on shear-induced particle migration, Cem. Concr. Res. 52 (2013) 216–224.
[19] G.R. Liu, M.B. Liu, Smoothed Particle Hydrodynamics, World Scientific Publishing Co. Pte Ltd, 2003.
[20] Z. Li, Z. Xu, R. Yoshioka, Flow simulation of fresh concrete using SPH method with consideration of geometry of particles, in: Sixth Int. Conf. Constr. Mater., Fukuoka, Japan, 2020, pp. 544–552.
[21] G. Cao, Z. Li, Z. Xu, A SPH simulation method for opening flow of fresh concrete considering boundary restraint, Constr. Build. Mater. 198 (2019) 379–389.
[22] W.S. Alyhya, S. Kulasegaram, B.L. Karihaloo, Simulation of the flow of self-compacting concrete in the V-funnel by SPH, Cem. Concr. Res. 100 (2017) 47–59.
[23] G. Cao, Z. Li, Numerical flow simulation of fresh concrete with viscous granular material model and smoothed particle hydrodynamics, Cem. Concr. Res. 100 (2017) 263–274.
[24] M.S. Abo Dhaheer, S. Kulasegaram, B.L. Karihaloo, Simulation of self-compacting concrete flow in the J-ring test using smoothed particle hydrodynamics (SPH), Cem. Concr. Res. 89 (2016) 27–34.
[25] S. Koshizuka, Y. Oka, Moving-Particle Semi-implicit method for fragmentation of incompressible fluid, Nucl. Sci. Eng. 123 (1996) 421–434.
[26] Y. Shimizu, H. Gotoh, A. Khayyer, An MPS-based particle method for simulation of multiphase flows characterized by high density ratios by incorporation of space potential particle concept, Comput. Math. Appl. 76 (2018) 1108–1129.
[27] Z. Xu, Z. Li, G. Cao, F. Jiang, Comparison of SPH and MPS methods for numerical flow simulations of fresh mortar, Proc. Japan Concr. Inst. 41 (2019) 1127–1132.
[28] J.J. Monaghan, On the problem of penetration in particle methods, J. Comput. Phys. 82 (1989) 1–15.
[29] Z. Xu, Z. Li, F. Jiang, The applicability of SPH and MPS methods to numerical flow simulation of fresh cementitious materials, Constr. Build. Mater. 274 (2021), 121736.
[30] H.D. Le, E.H. Kadri, S. Aggoun, J. Vierendeels, P. Troch, G. De Schutter, Effect of lubrication layer on velocity profile of concrete in a pumping pipe, Mater. Struct. 48 (2015) 3991–4003.
[31] Z. Xu, Z. Li, Numerical method for predicting flow and segregation behaviors of fresh concrete, Cem. Concr. Compos. 123 (2021), 104150.
[32] A. Khayyer, H. Gotoh, A 3D higher order Laplacian model for enhancement and stabilization of pressure calculation in 3D MPS-based simulations, Appl. Ocean Res. 37 (2012) 120–126.
[33] A. Khayyer, H. Gotoh, Development of CMPS method for accurate water-surface tracking in breaking waves, Coast. Eng. J. 50 (2008) 179–207.
[34] F. De Larrard, N. Roussel, Flow simulation of fresh concrete under a slipform machine, Road Mater. Pavement Des. 12 (2011) 547–566.
[35] S.N. Alekseev, On the calculation of resistance in pipe of concrete pumps, Mekhanizatia Storit. 9 (1952) 8–13.
[36] R. Weber, The Transport of Concrete by Pipeline, Cem. Concr. Assoc, London,UK, 1968.
[37] S.D. Jo, C.K. Park, J.H. Jeong, S.H. Lee, S.H. Kwon, A computational approach to estimating a lubricating layer in concrete pumping, Comput. Mater. Contin. 27 (2012) 189–210.
[38] T.T. Ngo, E.H. Kadri, R. Bennacer, F. Cussigh, Use of tribometer to estimate interface friction and concrete boundary layer composition during the fluid concrete pumping, Constr. Build. Mater. 24 (2010) 1253–1261.
[39] V.N. Nerella, V. Mechtcherine, Virtual sliding pipe rheometer for estimating pumpability of concrete, Constr. Build. Mater. 170 (2018) 366–377.

[40] D. Feys, A. Perez-Schell, R. Khatib, Development of a tribometer to characterize lubrication layer properties of self-consolidating concrete, Cem. Concr. Compos. 54 (2014) 40–52.
[41] S. Koshizuka, A. Nobe, Y. Oka, Numerical analysis of breaking waves using the moving particle semi-implicit method, Int. J. Numer. Methods Fluids 26 (1998) 751–769.
[42] H. Zhu, N.S. Martys, C. Ferraris, D. De Kee, A numerical study of the flow of Bingham-like fluids in two-dimensional vane and cylinder rheometers using a Smoothed Particle Hydrodynamics (SPH) based method, J. Nonnewton. Fluid Mech. 165 (2010) 362–375.
[43] T.C. Papanastasiou, Flows of materials with yield, J. Rheol. (N. Y. N. Y) 31 (1987) 385–404.
[44] A. Shakibaeinia, Y.C. Jin, MPS mesh-free particle method for multiphase flows, Comput. Methods Appl. Mech. Eng. 229–232 (2012) 13–26.
[45] G. Duan, B. Chen, S. Koshizuka, H. Xiang, Stable multiphase moving particle semi-implicit method for incompressible interfacial flow, Comput. Methods Appl. Mech. Eng. 318 (2017) 636–666.